

Strong Nonlinear Response in Crystalline Quartz at THz Frequencies

Soheil Zibod, Payman Rasekh, Murat Yildirim, Wei Cui, Ravi Bhardwaj, Jean-Michel Ménard, Robert W. Boyd, and Ksenia Dolgaleva*

This study reports on the experimental observation of a very strong nonlinear response in crystalline quartz in the terahertz (THz) frequency region through THz time-domain spectroscopy (THz-TDS). A previously established theoretical model is modified and presented and predicts a Kerr coefficient n_2 equal to $5.17 \times 10^{-14} \text{ m}^2 \text{ W}^{-1}$. The time-domain analysis of the measured data shows that with increasing of the THz peak amplitude, the pulse experiences a larger time delay in the sample. As the THz amplitude increases to values higher than 110 kV cm^{-1} , the growth rate of the delay decreases, indicating a saturation process. The value of the nonlinear refractive index calculated through the frequency-response analysis is estimated to be on the order of $10^{-13} \text{ m}^2 \text{ W}^{-1}$, which is several orders of magnitude larger than typical values of the nonlinear refractive index of solids in the visible region. Furthermore, a negative fifth-order susceptibility on the order of $10^{-30} \text{ m}^4 \text{ V}^{-4}$ is measured.

1. Introduction

Terahertz (THz) radiation, defined as a region of the electromagnetic spectrum between the microwaves and far-infrared, is gaining growing importance in applications such as biomedical sensing,^[1,2] security,^[3] spectroscopy, and imaging,^[4] and communications.^[5] Furthermore, THz time-domain spectroscopy (THz-TDS) systems are used for monitoring production

processes,^[6] art conservation,^[7] and characterization of materials.^[8]

THz-TDS allows the simultaneous measurement of the magnitude and phase of the THz signal through the linear electro-optic effect, representing a suitable technique for measuring the complex refractive index of a material at the THz frequencies.^[9] The recent development of intense THz pulse generation techniques opens the door to studying the nonlinear behavior of different materials in the THz region.^[10] Nonlinear effects such as THz-induced impact ionization and intervalley scattering in semiconductors,^[11–15] THz high-harmonic generation by hot carriers,^[16–19] and THz-induced ferroelectricity and collective coherence control have

been demonstrated.^[20,21] A very large third-order nonlinearity has been reported for water vapor,^[22] where the stepwise multiphoton transitions in water molecules lead to a third-order susceptibility of $\chi^{(3)} = (0.4 + 6i) \times 10^2 \text{ m}^2 \text{ V}^{-2}$. Extreme THz-induced Kerr effects have been reported for different liquids,^[23–27] where the nonlinear refractive indices can be several orders of magnitude larger than their values in the optical regime. The THz-induced Kerr effect has also been used to demonstrate the transient orientation of dipole moments in liquid water and the effect of cations and anions on the total polarizability anisotropy of aqueous ionic solutions.^[28,29] THz-induced Kerr effects have been observed in amorphous chalcogenide glasses such as arsenic trisulfide and arsenic triselenide.^[30] Kerr-like nonlinearity induced by a strong THz field has been reported in ZnTe, where the combination of THz generation and linear electro-optic effect reveals a THz-induced Kerr effect in optical frequencies using Z-scan technique.^[31] THz-induced Kerr-type birefringence has been investigated in the common optical window and substrate materials such as diamond, sapphire, and magnesium oxide in a THz pump-optical probe configuration.^[32] Z-cut quartz has also been explored and exhibits birefringence due to a linear electro-optic effect. Moreover, crystalline quartz has been used to efficiently generate intense broadband pulses and in broadband electro-optic sampling for frequencies up to 8 THz.^[33,34] Furthermore, it has been theoretically predicted that crystals can demonstrate an extremely large nonlinear refractive index at the THz frequency range.^[35] Crystalline solids such as quartz are expected to show THz nonlinear refractive indices that exceed the optical values by several orders of magnitude. Z-scan measurements of ZnSe crystal in THz frequencies have shown a nonlinear

S. Zibod, P. Rasekh, K. Dolgaleva
School of Electrical Engineering and Computer Science
University of Ottawa
Ottawa, Ontario K1N 6N5, Canada
E-mail: ksenia.dolgaleva@uottawa.ca

M. Yildirim, W. Cui, R. Bhardwaj, J.-M. Ménard, R. W. Boyd, K. Dolgaleva
Department of Physics
University of Ottawa
Ottawa, Ontario K1N 6N5, Canada
R. W. Boyd
Institute of Optics
University of Rochester
Rochester, New York 14627, United States

 The ORCID identification number(s) for the author(s) of this article can be found under <https://doi.org/10.1002/adom.202202343>

© 2023 The Authors. Advanced Optical Materials published by Wiley-VCH GmbH. This is an open access article under the terms of the Creative Commons Attribution-NonCommercial License, which permits use, distribution and reproduction in any medium, provided the original work is properly cited and is not used for commercial purposes.

DOI: 10.1002/adom.202202343

refractive index of $n_2 = 4 \times 10^{-11} \text{ cm}^2 \text{ W}^{-1}$.^[36] The majority of the works on the measurement of THz-induced nonlinear refractive index, using both the Z-scan technique and THz-TDS, are based on optical probe beams, resulting in the measurement of THz-induced third-order susceptibility in the form of $\chi^{(3)} = (\omega_{\text{opt}}, \omega_{\text{opt}}, \Omega_{\text{THz}}, -\Omega_{\text{THz}})$. Moreover, THz Z-scan is prone to error for thick samples.^[37] However, to the best of our knowledge, there has not been any experimental demonstration of THz-induced intensity-dependent refractive index using THz-TDS in a THz pump-THz probe measurement scheme reported to date.

Here, we report on the experimental observation of very strong nonlinear interactions in crystalline quartz in the THz regime.

First, a theoretical model for the nonlinear refractive index of quartz at the THz frequencies is presented.^[35] This model relies on the classical anharmonic oscillator, where the nonlinear refractive index is given as a sum of contributions from different vibrational modes. As predicted by the model, the value of the nonlinear refractive index at the lower frequencies exceeds its typical values in the visible range by several orders of magnitude. Then, we perform nonlinear THz-TDS on a 1-mm-thick z-cut quartz sample. The time-domain analysis of the collected data demonstrates an increased delay experienced by the pulse as it propagates through the sample with increasing THz beam intensity. However, the growth rate of the delay decreases with further intensity increase, revealing a phase saturation process. Further, the analysis in the Fourier domain shows an increase in the nonlinear phase and nonlinear absorption with the increase of the THz field intensity. At higher signal levels, however, the nonlinear phase grows with field intensity increase at a declining pace, whereas the nonlinear absorption tends to increase more rapidly. The data analysis revealed extremely large values of the nonlinear refractive index and fifth-order susceptibility, where the latter has a negative real part.

The manuscript is structured as follows: In Section 2, we describe a simple theoretical model for calculating the contributions from the vibrational modes to the nonlinear refractive index of crystalline quartz at THz frequencies, developed originally in Ref. [35]. We modify the model to include additional vibrational resonances, which helps us to achieve a better agreement with the experimental results. In Section 3, the experimental setup for the nonlinear THz-TDS is introduced. In Section 4, we present the experimental results. In addition to the time-domain analysis, the frequency response of crystalline quartz is presented. Finally, the nonlinear parameters of the material are calculated and the result is compared with the theoretical model.

2. Theory

An extremely large refractive index has been theoretically predicted for quartz in the THz regime, where the nonlinear refractive index was predicted to be several orders of magnitude larger than its typical visible and near-infrared values.^[35] The model is based on the equation of motion of a classical anharmonic oscillator:

$$\ddot{x} + 2\gamma\dot{x} + \omega_0^2 x + ax^2 + bx^3 = \alpha E \quad (1)$$

where x is the ion displacement from the equilibrium position, γ is damping factor, ω_0 is the resonance frequency, E is the ap-

plied field and a and b are the second- and third-order nonlinear coefficients, respectively. The parameter α on the right-hand side of Equation (1) is determined as $\alpha = q/m$, where q and m are the effective electric coupling strength and effective reduced mass of the vibrational mode, respectively. After applying perturbation theory and performing some algebraic operations,^[35] the relationship between the complex nonlinear refractive index and the resonance parameters takes the form

$$\tilde{n}_2 = \frac{\pi q N}{\tilde{n}_0} \frac{a^3}{(\omega_0^2 - \omega^2 - 2\gamma i \omega)^4} \times \left[2a^2 \frac{3\omega_0^2 - 8\omega^2 - 8\gamma i \omega}{\omega_0^2(\omega_0^2 - 4\omega^2 - 4\gamma i \omega)} + 3b \right] \quad (2)$$

Here N is the atomic density, and \tilde{n}_0 is the linear refractive index. Among the two terms, the term related to the second-order nonlinearity is two orders of magnitude larger than the contribution coming from the third-order nonlinear coefficient, b (see details in Supporting Information). This can be attributed to the fact that the cascaded processes are usually much stronger than the direct higher-order processes. The nonlinear coefficient a is related to the known parameters of the crystal through

$$a = -\frac{a_1 m \omega_0^4}{k_B} \alpha_T \quad (3)$$

where a_1 is the lattice constant, k_B is Boltzmann constant and α_T is the thermal expansion coefficient. With the assumption of a single dominant vibrational mode at 37.2 THz and ignoring the much weaker resonances at lower frequencies, one can evaluate the nonlinear refractive index of crystalline quartz at very low frequencies to be $\tilde{n}_2^{\omega \ll \omega_0} \approx 2.21 \times 10^{-9} \text{ esu}$ or, equivalently, $4.42 \times 10^{-16} \text{ m}^2 \text{ W}^{-1}$.^[35]

However, the strong vibrational resonance at 37.2 THz is not the only resonance contributing to the vibrational n_2 . There are several other resonances at lower frequencies, among which are the ones at 3.9 THz and 7.9 THz.^[38] To take the contribution of these additional resonances into consideration, we modify Equation (2) into the form

$$\tilde{n}_2 = \frac{\pi q N \alpha^3}{\tilde{n}_0} \sum_{j=1}^3 \frac{1}{(\omega_{0j}^2 - \omega^2 - 2\gamma i \omega)^4} \times \left[2a_j^2 \frac{3\omega_{0j}^2 - 8\omega^2 - 8\gamma i \omega}{\omega_{0j}^2(\omega_{0j}^2 - 4\omega^2 - 4\gamma i \omega)} + 3b_j \right] \quad (4)$$

In this modified equation, the nonlinear refractive index is now given as a sum of the contributions from the three resonances: the strong resonance at 37.2 THz, and the weaker resonances at 3.9 and 7.9 THz. Cross-interactions between the phonon resonances, as previously reported in the case of second-harmonic generation in the mid-infrared frequency range, could be considered to refine the theoretical model, but it is beyond the scope of this work.^[39] Equation (3) shows that the second-order nonlinear coefficient is proportional to ω_0^4 (see details in Supporting Information), meaning that the resonant value of the nonlinear coefficient for the dominant resonance is, for instance, approximately

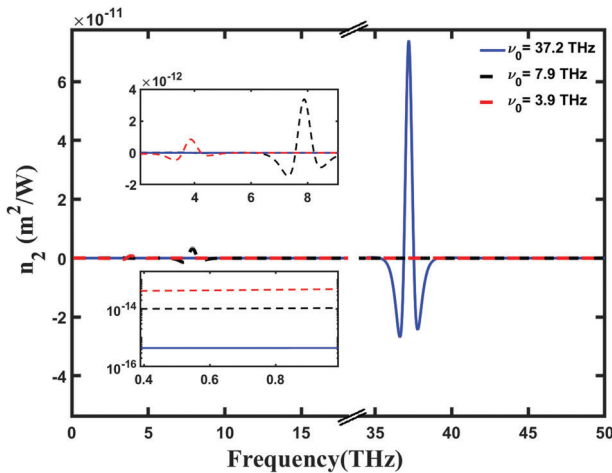


Figure 1. Theoretical modelling of the nonlinear refractive index caused by the dominant resonance at 37.2 THz (blue solid lines) and the resonances at 7.9 THz (black dashed lines) and 3.9 THz (red dashed lines) in quartz. The top inset resolves the values of the nonlinear refractive indices at around the low-frequency resonances. The bottom inset shows the contribution from three resonances at the lower frequencies (1 THz and lower).

Table 1. The contribution to the nonlinear refractive index.

ω_0 (THz)	$n_2^{\omega \ll \omega_0}$ ($\text{m}^2 \text{W}^{-1}$)	$n_2^{\omega \approx \omega_0}$ ($\text{m}^2 \text{W}^{-1}$)
3.9	4.17×10^{-14}	8.38×10^{-13}
7.9	9.98×10^{-15}	3.35×10^{-12}
37.2	4.42×10^{-16}	7.40×10^{-11}

500 times larger than that for the resonance at 7.9 THz. **Figure 1** shows the dispersion of the nonlinear refractive index caused by the dominant resonance and the resonances at 7.9 and 3.9 THz. The top inset of **Figure 1** resolves the value of n_2 at around low-frequency resonances. The comparison indicates that the nonlinear refractive index at the dominant resonance at 37.2 THz is approximately 20 times larger than the one at the stronger resonance of the two lower-frequency resonances.

Substituting Equation (3) into Equation (4), we can see that the contributions of different resonances to the nonlinear refractive index at very low frequencies are proportional to $1/\omega_0^2$. Consequently, at much lower frequencies (1 THz and below), the contributions from the resonances at 7.9 and 3.9 THz are approximately 20 times larger and 100 times larger than the one at 37.2 THz, respectively, as shown in the bottom inset of **Figure 1**. The contributions of the three resonances to the nonlinear refractive index are listed in **Table 1**. The table clearly demonstrates that the dominant contributions to the nonlinear refractive index at very low frequencies are from the resonances at 7.9 and 3.9 THz: $n_2^{\omega \ll \omega_0} \approx 5.17 \times 10^{-14} \text{ m}^2 \text{W}^{-1}$.

3. Experimental Section

The intense THz radiation was generated in an optical rectification process in lithium niobate (LiNbO_3), where the pulse-front tilting technique was used to make the process phase-matched and efficient.^[10] The setup schematic was depicted in **Figure 2**.

The beam, coming from a 800-nm Ti:sapphire laser with a pulse duration of 45 fs and repetition rate of 1 kHz, was split into the pump and probe paths. In the pump path, the beam diffracts from a grating and, after passing through two cylindrical lenses, propagates through the generation crystal. The generated THz radiation was collimated and focused with several gold off-axis parabolic mirrors. A pair of wire-grid polarizers was also used to control the THz field amplitude during the measurements.

In the probe path, the near-infrared (NIR) probe and THz beams co-propagated inside the 200- μm -thick ZnTe detection crystal. A delay stage was also used to change the overlap time between the THz and probe beams, so that one could measure different points of the THz pulse. As the THz pulse propagated through the detection crystal, the refractive index experienced by the probe beam was modified through the linear electro-optic effect, resulting in a birefringence in the crystal. The phase difference induced by the birefringence is then converted into the beam's ellipticity via a quarter-wave plate. A Wollaston prism split the beam into two components of which their intensity difference was proportional to the beam ellipticity. Finally, a pair of balanced photodetectors connected to the lock-in amplifier was used to detect the differential signal. The peak amplitude of the electric field was estimated to be 225 kV cm^{-1} at the focal position where the 1-mm z-cut quartz sample was placed. To eliminate the water-vapor absorption, the part of the setup where the THz beam was generated and propagated was enclosed and purged with nitrogen. Different field amplitudes were obtained by rotating the first wire-grid polarizer and keeping the second one fixed.

4. Results and Discussion

In **Figure 3a**, we show the time-domain signals for different THz field amplitudes for both free-space and crystalline quartz. One can observe an increase in the time delay experienced by the pulse in the crystal quartz with an increase of the THz field amplitude. The inset in **Figure 3** clearly demonstrates this observation. In contrast, the free-space THz time-domain signal does not exhibit such a delay increase.

Figure 3b shows the average time shift for each of the THz field amplitude levels compared to the lowest-level amplitude, where the average time shift for each level is calculated as

$$t_{\text{av}}^i = \frac{1}{N} \sum_k^N t(V_i = V_k) - t(V_{\text{low}} = V_k) \quad (5)$$

Here t_{av}^i is the average time shift, N is the number of data points, V_i is the i -th signal and V_{low} is the lowest-level signal. The analysis is performed over the main lobe, the interval between the first two minima, highlighted in the inset of **Figure 3a**, as it represents most of the THz spectral content. We can see that, with the field intensity increase, THz pulse experiences more delay with respect to the lowest-intensity pulse. However, at higher intensities, the growth slope declines, which indicates the presence of the saturation effect. From the pulse duration of $\tau_d \approx 2.5$ ps, one can estimate the nonlinear refractive index by approximating the signal with its main frequency component $f \approx 1/\tau_d = 0.4$ THz. We can relate the nonlinear refractive index to the slope of the linear region of the figure through $n_2 = (\Delta t_{\text{av}}/\Delta I)cd^{-1}$, where $d = 1$ mm

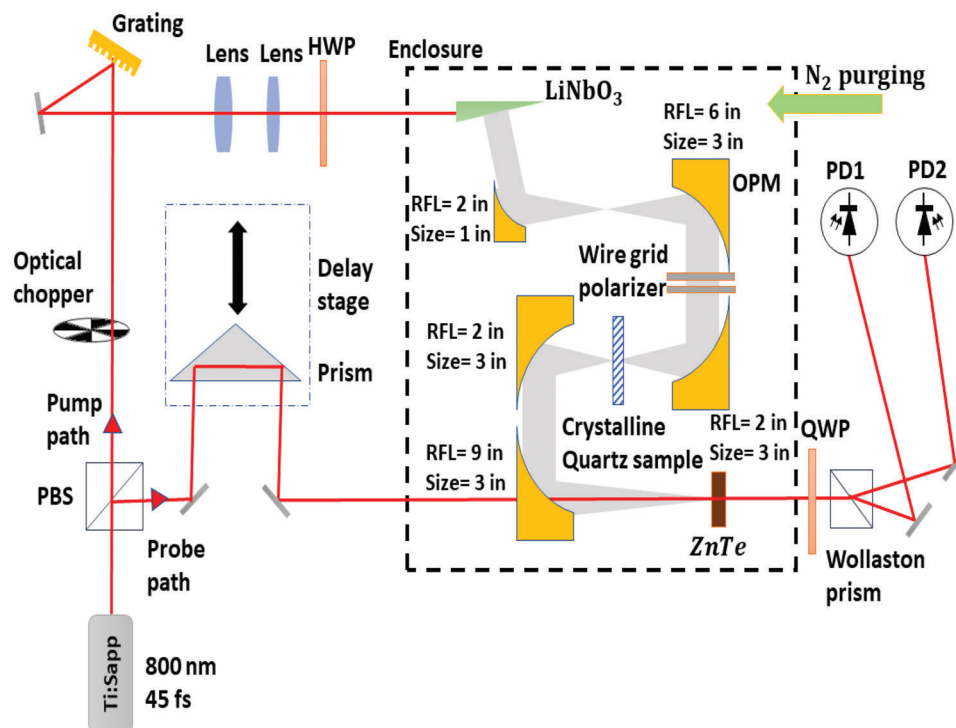


Figure 2. The schematic of THz-TDS experimental setup. The 800-nm beam is split into pump and probe paths. The phase-matching condition required for the generation of intense THz field in LiNbO₃ crystal is achieved through the pulse-front tilting technique. OPM: Off-axis parabolic mirror; HWP: Half-wave plate; QWP: Quarter-wave plate; PD: Photodetector; RFL: Reflective focal length.

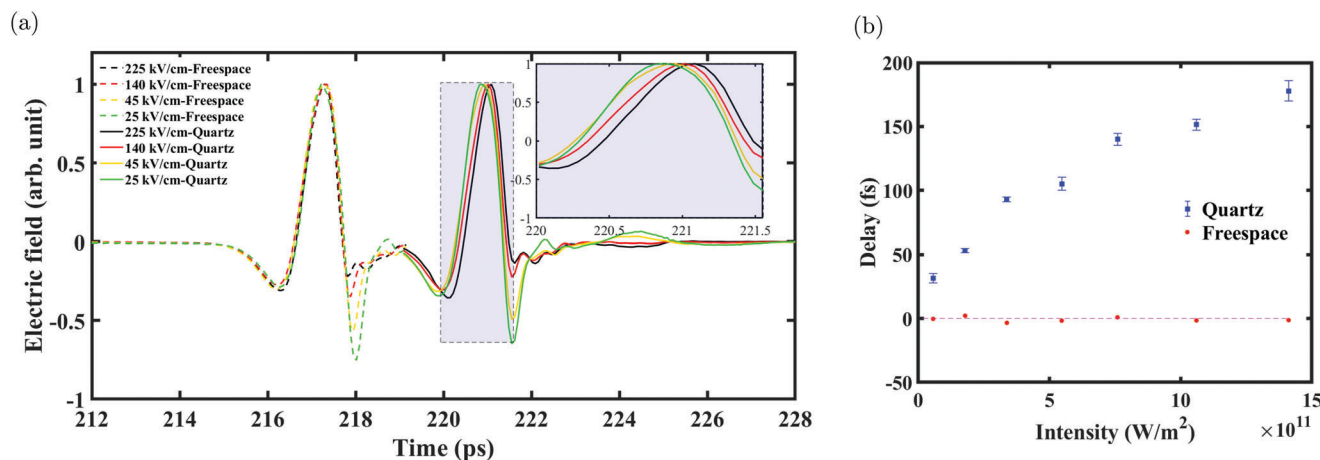


Figure 3. a) THz time-domain signal in free space (dashed lines) and crystalline quartz (solid lines) for different signal levels. The inset shows the delay increase with the growth of the THz amplitude. b) The average time shift in free space (red) and in crystalline quartz (blue) for different signal levels.

is the thickness of the sample. Thus, the nonlinear refractive index is calculated to be $n_2 = 7.5 \times 10^{-14} \text{ m}^2 \text{ W}^{-1}$. At higher intensities, the saturation effect limits the refractive index change, reducing the nonlinear refractive index to smaller values. Thus, the delay increases at a slower pace with the further increase of the intensity.

Figure 4a shows the spectral density for the quartz sample and free space in the frequency range between 0.3 and 2 THz, where the fast Fourier transform (FFT) performed on the time-domain

signal is depicted (see more details in Supporting Information). We notice that as the signal level increases, the absorption, which is the difference between the free-space and quartz sample spectra after factoring out the sample's Fresnel reflections, increases. This behavior clearly indicates the presence of a nonlinear absorption process.

Figure 4b shows the nonlinear phase experienced by the THz signal for different intensity levels at 0.4 THz where the spectral density is maximum. It indicates that, as the THz intensity

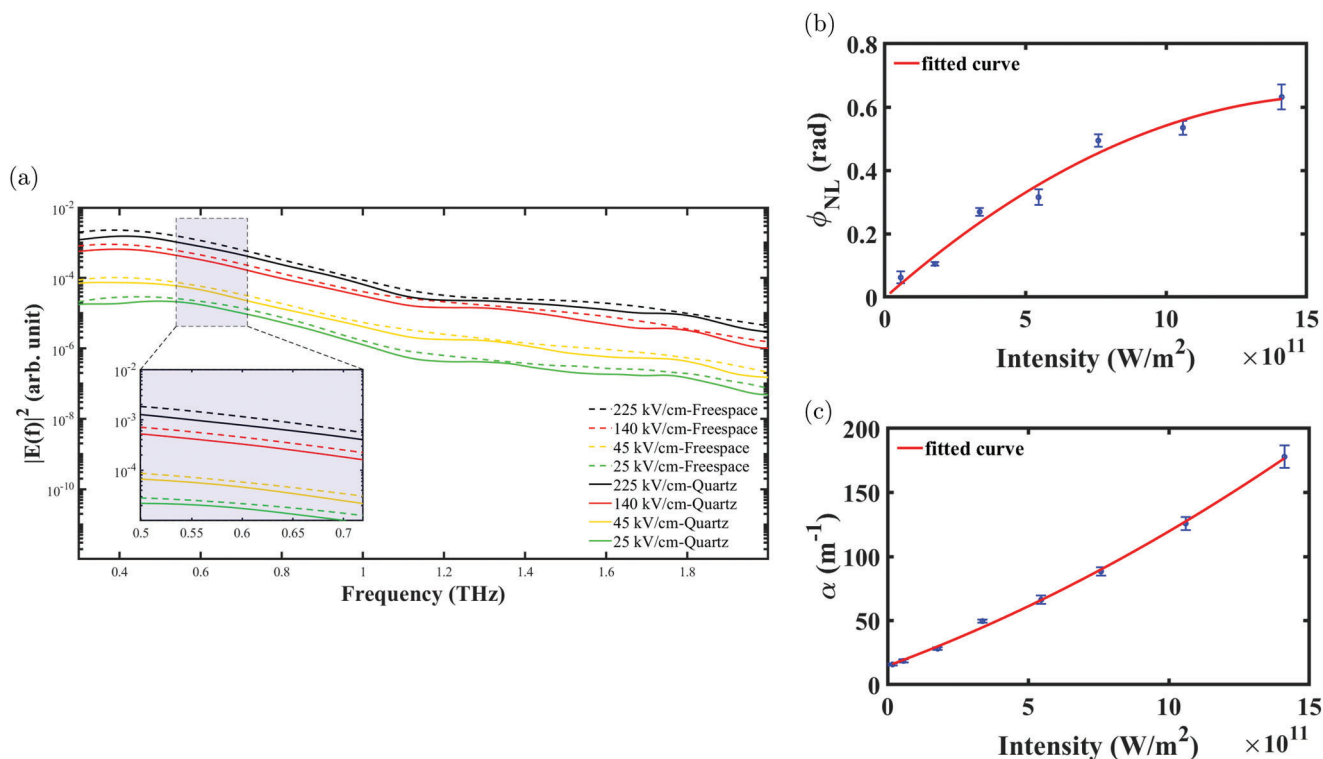


Figure 4. a) Signal spectral density for free-space (dashed lines) and quartz (solid lines). The difference between the free-space and quartz signals increases with an increase in the signal level. b) nonlinear phase experienced by the signal of different amplitude at 0.4 THz. c) absorption coefficient for each signal level at 0.4 THz.

increases, the nonlinear phase cannot be expressed with a single nonlinear term and suggests a negative higher-order nonlinearity term. Z-cut quartz is a non-centrosymmetric crystal, meaning that both the even- and odd-order susceptibilities are nonzero. However, the even-order nonlinearities are not of direct relevance in this study, as we are interested in exploring the nonlinearities at the fundamental frequency. Nevertheless, the even-order nonlinearities can contribute to the self-action effects in a cascaded manner.^[35] The differential nonlinear phase for the higher THz field amplitudes in a sample with a thickness of d is related to the intensity by

$$\phi_i^{NL}(\omega) = \phi_i(\omega) - \phi_{low}(\omega) = n_2(\omega)I_i \frac{\omega}{c} d + n_4(\omega)I_i^2 \frac{\omega}{c} d \quad (6)$$

Here ϕ_i is the total phase of the i -th signal and ϕ_{low} is the phase experienced by the lowest-level signal, used as the linear response of the material, n_2 and n_4 are the second-order and fourth-order nonlinear refractive indices, respectively, and I_i is the peak intensity of the i -th level signal. By observation of Figure 4b, one can conclude that a negative n_4 effect is likely to be contributing to the intensity dependence of the nonlinear phase shift.

The absorption coefficient of crystalline quartz, measured as a function of the THz intensity, is depicted in Figure 4c (see details in Supporting Information). We can see that at lower intensities, the absorption coefficient increases linearly with respect to the

field intensity. However, at higher intensities, a quadratic term also reveals itself. The absorption coefficient of the material can be expressed as

$$\alpha(\omega) = \alpha_0(\omega) + \alpha_2(\omega)I_i + \alpha_4(\omega)I_i^2 \quad (7)$$

where α , α_0 , α_2 , and α_4 are total absorption coefficient, linear absorption coefficient, two-photon absorption coefficient, and three-photon absorption coefficient, respectively. We calculate the value of n_2 to be $n_2 = (9.0 \pm 1.4) \times 10^{-14} m^2 W^{-1}$. This value is 20% greater than the value estimated from the time-domain analysis for n_2 at 0.4 THz as the main frequency component of the signal. This difference is potentially rooted in approximating the signal with a single-frequency component. In fact, the frequencies with lower amplitudes experience smaller nonlinear delay and reduce the average time shift calculated in the time domain. Furthermore, the measured value exceeds the theoretically predicted value by a factor of 1.74. This difference arises from the fact that the theoretical calculations carried out were based on the assumption that the field is monochromatic. However, the THz field used in the experiment is a short wide-band pulse. Consequently, there are contributions to the nonlinear phase shift at 0.4 THz from different frequencies, resulting in the higher value of ϕ^{NL} . Furthermore, the data analysis reveals the values of other nonlinear coefficients: $n_4 = (-2.7 \pm 1.0) \times 10^{-26} m^4 W^{-2}$, $\alpha_2 = (8.1 \pm 0.9) \times 10^{-11} m W^{-1}$ and $\alpha_4 = (2.4 \pm 0.6) \times 10^{-23} m^3 W^{-2}$.

The real and imaginary parts of third-order and fifth-order nonlinear susceptibility are related to these nonlinear coefficients as:

$$\Re(\chi^{(3)}) = \frac{4}{3} n_0^2 \epsilon_0 c n_2 \quad (8a)$$

$$\Im(\chi^{(3)}) = \frac{2}{3} n_0^2 \epsilon_0 \frac{c^2}{\omega} \alpha_2 \quad (8b)$$

$$\Re(\chi^{(5)}) = \frac{8}{5} n_0^3 \epsilon_0^2 c^2 n_4 \quad (8c)$$

$$\Im(\chi^{(5)}) = \frac{4}{5} n_0^3 \epsilon_0^2 \frac{c^3}{\omega} \alpha_4 \quad (8d)$$

Thus, the complex third-order and fifth-order nonlinear susceptibility are found as $\chi^{(3)} = (1.4 \times 10^{-15} + i7.5 \times 10^{-17}) \text{ m}^2 \text{ V}^{-2}$ and $\chi^{(5)} = (-2.7 \times 10^{-30} + i1.5 \times 10^{-31}) \text{ m}^4 \text{ V}^{-4}$, respectively. These measurements confirm the presence of an extremely large nonlinear refractive index at lower THz frequencies. This extreme behavior agrees with the theoretical modelling presented in Section 2 for the lower frequency regime. However, in order to examine the presented model in a wide spectrum, especially in the vicinity of the phonon resonances, one may need to excite the sample at these frequencies, which are beyond the spectral range provided by our source. Sources based on DAST organic crystals or two-color air plasma generation can be used to cover a wider spectral range. Another challenge that requires a special treatment when pumping at the resonance frequencies is the strong absorption that may prevent the observation of any signal. Moreover, the absorption rapidly reduces the field strength, preventing the propagation of the nonlinear driving field. As a solution to this challenge, one may need to convert the setup to a reflection geometry as implemented previously for the case of the second-harmonic generation in quartz at the THz frequencies.^[39]

5. Conclusion

We observe a strong nonlinear response of crystalline quartz in the THz region. The experimental results confirm the theoretical predictions made earlier, with an amendment to the theory by including additional vibrational resonances.

Further, time-domain spectroscopy reveals that the observed nonlinear behavior results from a complex interplay of the third- and fifth-order susceptibilities, where the real part shows a positive third-order and a negative fifth-order contribution. Furthermore, the measured nonlinear refractive index of $n_2 = 9.0 \times 10^{-14} \text{ m}^2 \text{ W}^{-1}$ at 0.4 THz is seven orders of magnitude larger than the nonlinear refractive index of fused silica measured in the visible region. We attribute this large nonlinearity to the contributions from the vibrational modes in the crystal. Numerical evaluation of Equation (4) reveals that the vibrational modes at 3.9 and 7.9 THz are the primary contributions to this large nonlinear response, despite the fact that the strong resonance at 37.2 THz might be expected to be the origin of the large optical nonlinearity. Including these lower-frequency resonances allowed us to obtain a correct order-of-magnitude agreement between the theory and experiment. The slight difference in the values of the measured and predicted n_2 (a factor of 1.74) is rooted in the fact

that the spectrum of the THz radiation is wide-band, and the contribution of different spectral components is possible. This difference is a motivation for future exploration aimed at pushing the analysis beyond the approximation of monochromatic radiation – the necessary measure in the extremely wide-band THz frequency range.

Supporting Information

Supporting Information is available from the Wiley Online Library or from the author.

Acknowledgements

The authors acknowledge support from the Canada Research Chairs program and Natural Science and Engineering Council's Strategic program STGP 521619. RWB acknowledges support through the Natural Sciences and Engineering Research Council of Canada, the Canada Research Chairs program, by US DARPA award W911NF-18-1-0369, US ARO award W911NF-18-1-0337, and a US Office of Naval Research MURI award N00014-20-1-2558. The authors are thankful to Prof. Eric VanStryland for fruitful discussion.

Conflict of Interest

The authors declare no conflict of interest.

Data Availability Statement

The data that support the findings of this study are available from the corresponding author upon reasonable request.

Keywords

crystal quartz, nonlinear refractive index, THz radiation, vibrational modes

Received: October 4, 2022

Revised: May 2, 2023

Published online:

- [1] Y. Peng, C. Shi, X. Wu, Y. Zhu, S. Zhuang, *BME Front.* **2020**, 2020, 2547609.
- [2] H. Lindley-Hatcher, R. I. Stantchev, X. Chen, A. I. Hernandez-Serrano, J. Hardwicke, E. Pickwell-MacPherson, *Appl. Phys. Lett.* **2021**, 118, 230501.
- [3] J. Chen, Y. Chen, H. Zhao, G. J. Bastiaans, X.-C. Zhang, *Opt. Express* **2007**, 15, 12060.
- [4] P. Jepsen, D. Cooke, M. Koch, *Laser Photonics Rev.* **2011**, 5, 124.
- [5] T. Kleine-Ostmann, T. Nagatsuma, *J. Infrared Millim. Terahertz Waves.* **2011**, 32, 143.
- [6] N. Krumbholz, T. Hochrein, N. Vieweg, T. Hasek, K. Kretschmer, M. Bastian, M. Mikulics, M. Koch, *Polym. Test.* **2009**, 28, 30.
- [7] K. Krügener, M. Schwerdtfeger, S. F. Busch, A. Soltani, E. Castro-Camus, M. Koch, W. Viöl, *Sci. Rep.* **2015**, 5, 14842.
- [8] S. Busch, M. Weidenbach, M. Fey, F. Schäfer, T. Probst, M. Koch, *J. Infrared Millim. Terahertz Waves.* **2014**, 35, 993.
- [9] A. Nahata, D. H. Auston, T. F. Heinz, C. Wu, *Appl. Phys. Lett.* **1996**, 68, 150.

- [10] J. Hebling, K.-L. Yeh, M. C. Hoffmann, B. Bartal, K. A. Nelson, *J. Opt. Soc. Am. B* **2008**, *25*, B6.
- [11] S. Ašmontas, S. Bumelienė, J. Gradauskas, R. Raguotis, A. Sužiedėlis, *Sci. Rep.* **2020**, *10*, 10580.
- [12] M. C. Hoffmann, J. Hebling, H. Y. Hwang, K.-L. Yeh, K. A. Nelson, *Phys. Rev. B* **2009**, *79*, 161201.
- [13] C. Lange, T. Maag, M. Hohenleutner, S. Baierl, O. Schubert, E. R. J. Edwards, D. Bougeard, G. Woltersdorf, R. Huber, *Phys. Rev. Lett.* **2014**, *113*, 227401.
- [14] A. T. Tarekgegne, K. Iwaszczuk, M. Zalkovskij, A. C. Strikwerda, P. U. Jepsen, *J. Phys.* **2015**, *17*, 043002.
- [15] S. Tani, F. m. c. Blanchard, K. Tanaka, *Phys. Rev. Lett.* **2012**, *109*, 166603.
- [16] O. Schubert, M. Hohenleutner, F. Langer, B. Urbanek, C. Lange, U. Huttner, D. Golde, T. Meier, M. Kira, S. W. Koch, R. Huber, *Nat. Photonics* **2014**, *8*, 119.
- [17] H. A. Hafez, S. Kovalev, J.-C. Deinert, Z. Mics, B. Green, N. Awari, M. Chen, S. Germanskiy, U. Lehnert, J. Teichert, Z. Wang, K.-J. Tielrooij, Z. Liu, Z. Chen, A. Narita, K. Müllen, M. Bonn, M. Gensch, D. Turchinovich, *Nature* **2018**, *561*, 507.
- [18] X. Chai, X. Ropagnol, S. M. Raeis-Zadeh, M. Reid, S. Safavi-Naeini, T. Ozaki, *Phys. Rev. Lett.* **2018**, *121*, 143901.
- [19] P. Gaal, K. Reimann, M. Woerner, T. Elsaesser, R. Hey, K. H. Ploog, *Phys. Rev. Lett.* **2006**, *96*, 187402.
- [20] T. Qi, Y.-H. Shin, K.-L. Yeh, K. A. Nelson, A. M. Rappe, *Phys. Rev. Lett.* **2009**, *102*, 247603.
- [21] X. Li, T. Qiu, J. Zhang, E. Baldini, J. Lu, A. M. Rappe, K. A. Nelson, *Science* **2019**, *364*, 1079.
- [22] P. Rasekh, A. Safari, M. Yildirim, R. Bhardwaj, J.-M. Ménard, K. Dolgaleva, R. W. Boyd, *ACS Photonics* **2021**, *8*, 1683.
- [23] A. Tcypkin, M. Zhukova, M. Melnik, I. Vorontsova, M. Kulya, S. Putilin, S. Kozlov, S. Choudhary, R. W. Boyd, *Phys. Rev. Appl.* **2021**, *15*, 054009.
- [24] M. C. Hoffmann, N. C. Brandt, H. Y. Hwang, K.-L. Yeh, K. A. Nelson, *Appl. Phys. Lett.* **2009**, *95*, 231105.
- [25] A. N. Tcypkin, M. V. Melnik, M. O. Zhukova, I. O. Vorontsova, S. E. Putilin, S. A. Kozlov, X.-C. Zhang, *Opt. Express* **2019**, *27*, 10419.
- [26] K. J. G. Francis, M. L. P. Chong, Y. E, X.-C. Zhang, *Opt. Lett.* **2020**, *45*, 5628.
- [27] M. Zhang, W. Xiao, C. Zhang, L. Zhang, *Sensors* **2022**, *22*, 23.
- [28] P. Zalden, L. Song, X. Wu, H. Huang, F. Ahr, O. D. Mücke, J. Reichert, M. Thorwart, P. K. Mishra, R. Welsch, R. Santra, F. X. Kärtner, C. Bressler, *Nat. Commun.* **2018**, *9*, 2142.
- [29] V. Balos, N. K. Kaliannan, H. Elgabarty, M. Wolf, T. D. Kühne, M. Sajadi, *Nat. Chem.* **2022**, *14*, 1031.
- [30] M. Zalkovskij, A. C. Strikwerda, K. Iwaszczuk, A. Popescu, D. Savastru, R. Malureanu, A. V. Lavrinenko, P. U. Jepsen, *Appl. Phys. Lett.* **2013**, *103*, 221102.
- [31] W.-Q. He, C.-M. Gu, W.-Z. Shen, *Opt. Express* **2006**, *14*, 5476.
- [32] M. Sajadi, M. Wolf, T. Kampfrath, *Opt. Express* **2015**, *23*, 28985.
- [33] Y. Wei, J. Le, L. Huang, C. Tian, *Appl. Phys. Lett.* **2023**, *122*, 081105.
- [34] V. Balos, M. Wolf, S. Kovalev, M. Sajadi, *Opt. Express* **2023**, *31*, 13317.
- [35] K. Dolgaleva, D. V. Materikina, R. W. Boyd, S. A. Kozlov, *Phys. Rev. A* **2015**, *92*, 023809.
- [36] A. N. Tcypkin, S. E. Putilin, M. S. Kulya, M. Siddiqui, S. Choudhary, J. Zhao, V. G. Bespalov, R. Boyd, X. C. Zhang, S. A. Kozlov, in *2017 42nd International Conference on Infrared, Millimeter, and Terahertz Waves (IRMMW-THz)*, **2017**, pp. 1–1.
- [37] M. Melnik, I. Vorontsova, S. Putilin, A. Tcypkin, S. Kozlov, *Sci. Rep.* **2019**, *9*, 9146.
- [38] C. L. Davies, J. B. Patel, C. Q. Xia, L. M. Herz, M. B. Johnston, *J. Infrared Millim. Terahertz Waves.* **2018**, *39*, 1236.
- [39] C. J. Winta, S. Gewinner, W. Schöllkopf, M. Wolf, A. Paarmann, *Phys. Rev. B* **2018**, *97*, 094108.

ADVANCED OPTICAL MATERIALS

Supporting Information

for *Adv. Optical Mater.*, DOI 10.1002/adom.202202343

Strong Nonlinear Response in Crystalline Quartz at THz Frequencies

*Soheil Zibod, Payman Rasekh, Murat Yildirim, Wei Cui, Ravi Bhardwaj, Jean-Michel Ménard, Robert W. Boyd and Ksenia Dolgaleva**

Supporting information

Extremely large nonlinear response in crystalline quartz at THz frequencies

Soheil Zibod* Payman Rasekh Murat Yildirim Wei Cui Ravi Bhardwaj Jean-Michel Ménard Robert W. Boyd Ksenia Dolgaleva

This document provides supplementary information for "Extremely large nonlinear response in crystalline quartz at THz frequencies". We present a more detailed derivation from Ref. ^[1] and the modification to this model, presented in this work. We also include a numerical simulation of the nonlinear absorption. In the end, we present additional detail about the data analysis.

Theoretical model:

The theoretical modeling starts with anharmonic oscillator as described in Ref. ^[1]:

$$\ddot{x} + 2\gamma\dot{x} + \omega_0^2x + ax^2 + bx^3 = \alpha E, \quad (\text{S1})$$

where x is the ion displacement from the equilibrium position, γ is the damping factor, ω_0 is the resonance frequency, E is the applied field and a and b are the second- and third-order nonlinear coefficients, respectively. The parameter α on the right-hand side of Equation (S1) is determined as $\alpha = q/m$, where q and m are the effective electric coupling strength and effective reduced mass of the vibrational mode, respectively. Applying perturbation theory and introducing the expansion parameter $0 \leq \lambda \leq 1$, we sort and split the terms with respect to the power of λ into three equations:

$$\ddot{x}^{(1)} + 2\gamma\dot{x}^{(1)} + \omega_0^2x^{(1)} = \alpha E, \quad (\text{S2a})$$

$$\ddot{x}^{(2)} + 2\gamma\dot{x}^{(2)} + \omega_0^2x^{(2)} + a[x^{(1)}]^2 = 0, \quad (\text{S2b})$$

$$\ddot{x}^{(3)} + 2\gamma\dot{x}^{(3)} + \omega_0^2x^{(3)} + 2ax^{(1)}x^{(2)} + b[x^{(1)}]^3 = 0. \quad (\text{S2c})$$

Equation (S2a) gives the expression related to linear response, while Equation (S2b) describes the second-order nonlinear processes. Equation (S2c) describes the third-order nonlinear phenomena, including intensity-dependent refractive index, which is the process of interest in this work. Assuming a monochromatic field, we can calculate the third-order nonlinear ion displacement at the fundamental frequency ω as

$$x_\omega^{(3)} = \frac{\alpha^3}{(\omega_0^2 - \omega^2 - 2\gamma i\omega)^4} \times \left[2a^2 \frac{3\omega_0^2 - 8\omega^2 - 8\gamma i\omega}{\omega_0^2(\omega_0^2 - 4\omega^2 - 4\gamma i\omega)} + 3b \right] |E_\omega|^2 E. \quad (\text{S3})$$

The polarization and displacement are related through $P = Nqx$. The polarization at the fundamental frequency can be expressed as the sum of the linear term and the nonlinear term as $P_\omega = \chi^{(1)}E_\omega + 3\chi^{(3)}|E_\omega|^2E_\omega$, where the third-order nonlinear susceptibility $\chi^{(3)}$ is given by

$$\chi^{(3)} = \frac{qN}{3} \frac{\alpha^3}{(\omega_0^2 - \omega^2 - 2\gamma i\omega)^4} \times \left[2a^2 \frac{3\omega_0^2 - 8\omega^2 - 8\gamma i\omega}{\omega_0^2(\omega_0^2 - 4\omega^2 - 4\gamma i\omega)} + 3b \right]. \quad (\text{S4})$$

Finally, the complex nonlinear refractive index is calculated as

$$\tilde{n}_2 = \frac{3\pi\chi^{(3)}}{\tilde{n}_0} = \frac{\pi qN}{\tilde{n}_0} \frac{\alpha^3}{(\omega_0^2 - \omega^2 - 2\gamma i\omega)^4} \times \left[2a^2 \frac{3\omega_0^2 - 8\omega^2 - 8\gamma i\omega}{\omega_0^2(\omega_0^2 - 4\omega^2 - 4\gamma i\omega)} + 3b \right]. \quad (\text{S5})$$

As one can see from Eq. (S5), there are two terms contributing to the complex nonlinear refractive index: the term related to the second-order nonlinear coefficient a and the other one related to the third-order nonlinear coefficient b . Under the assumption of a single dominant resonance at 37.2 THz for

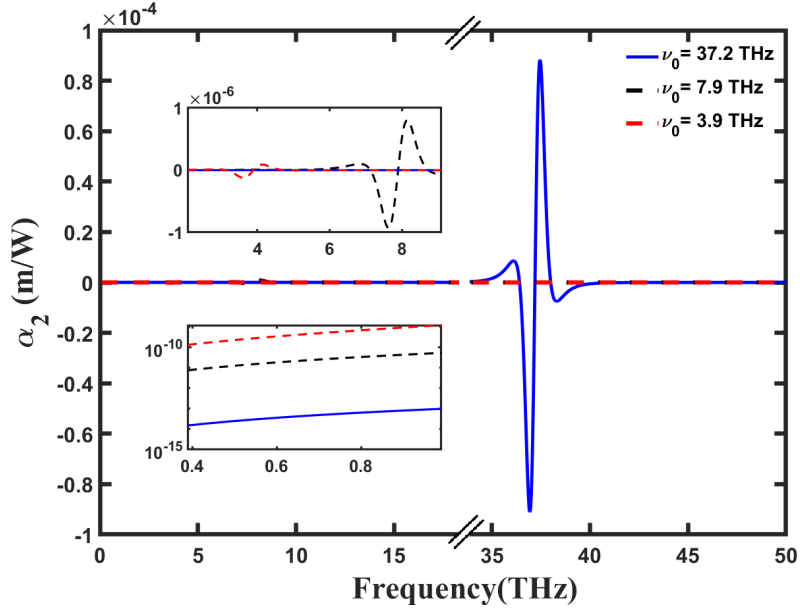


Figure S1: Theoretical modelling of the nonlinear absorption coefficient caused by the dominant resonance at 37.2 THz (blue solid lines) and the resonances at 7.9 THz (black dashed lines) and 3.9 THz (red dashed lines) in quartz. The top inset resolves the values of the nonlinear absorption coefficient at around low-frequency resonances. The bottom inset shows the contribution from the three resonances at the lower frequencies (1 THz and lower).

quartz,^[1] one can evaluate the first and second contribution as $n_{2\nu_1} = 4.48 \times 10^{-16} \text{ m}^2 \text{ W}^{-1}$ and $n_{2\nu_2} = -6.54 \times 10^{-18} \text{ m}^2 \text{ W}^{-1}$, respectively. It follows from the estimate that the contribution from the cascaded second-order process is approximately two orders of magnitude larger than the one from the direct third-order process.

The factor other than the resonance frequency in the calculation of a and b coefficients is the contribution of each resonance to the susceptibility at low frequencies. The assumption was that a small part of the susceptibility comes from electronic resonances in optical regime, and the rest comes from the dominant resonance at 37.2 THz. However, the Sellmeier's equation for quartz is as follows:^[2]

$$n^2 - 1 = \frac{0.6961663\lambda^2}{\lambda^2 - 0.0684043^2} + \frac{0.4079426\lambda^2}{\lambda^2 - 0.1162414^2} + \frac{0.8974794\lambda^2}{\lambda^2 - 9.896161^2}. \quad (\text{S6})$$

The first two contributions come from the UV resonances and the third one is from the dominant THz resonance. The sum of these three contributions [the right-hand side of Eq. (S6) as is] is approximately equal to 2. However, assuming the known value of the low-frequency refractive index of quartz to be $n = 2.1$ ^[3], we obtain $n^2 - 1 = 2.1^2 - 1 = 3.4$, which differs from 2 by 1.4. It is known that there are additional low-frequency resonances that are associated with crystal quartz that must be responsible for the remaining 1.4.^[4] As a result, the a and b coefficients can be expressed as the functions of the resonance frequency.

The second-order nonlinear coefficient is proportional to ω_0^4 . Therefore, we can calculate the relation between the nonlinear refractive index and the resonance frequency ω_0 at two frequency regions: at resonance and at very low frequencies. The expressions at these two limits are:

$$\tilde{n}_2 \Big|_{\omega=\omega_0} \propto \frac{1}{\omega_0^4} \times \left[\omega_0^8 \frac{\omega_0^2}{\omega_0^2(\omega_0^2)} \right] \propto \omega_0^2, \quad (\text{S7a})$$

$$\tilde{n}_2 \Big|_{\omega \ll \omega_0} \propto \frac{1}{\omega_0^8} \times \left[\omega_0^8 \frac{\omega_0^2}{\omega_0^2(\omega_0^2)} \right] \propto \omega_0^{-2}. \quad (\text{S7b})$$

One can conclude that while the value of nonlinear refractive index at the dominant resonance is much larger than its value at a much smaller resonance close to the low-frequency regime, the latter plays the dominant role in the low-frequency regime, as shown in the Table (1) of the main text. Thus, Equation

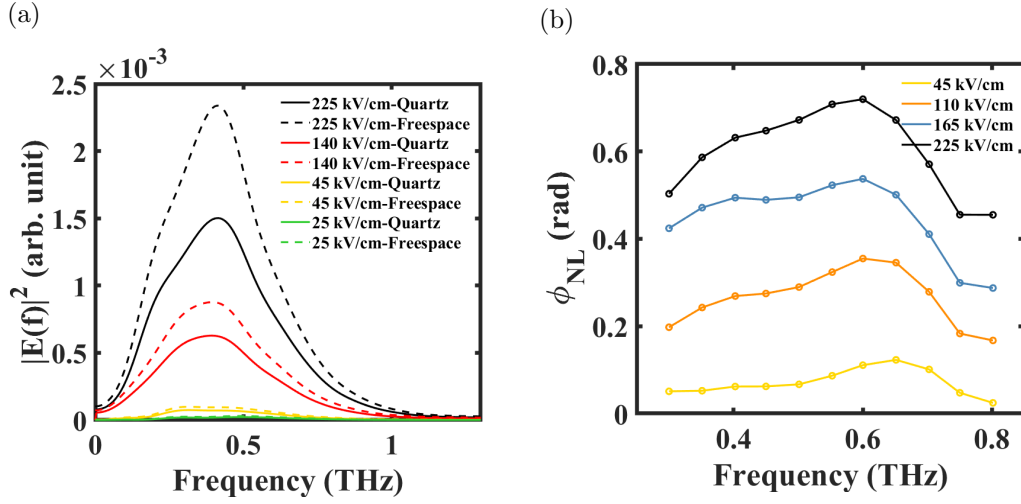


Figure S2: (a) THz signal spectral density for free-space (dashed lines) and quartz (solid lines). (b) nonlinear phase experienced by the signal of different amplitude.

(S5) should be modified as a sum of contributions from the dominant resonance at 37.2 THz and much smaller resonances at 7.9 THz and 3.9 THz:

$$\tilde{n}_2 = \frac{\pi q N \alpha^3}{\tilde{n}_0} \sum_{j=1}^3 \frac{1}{(\omega_{0,j}^2 - \omega^2 - 2\gamma i \omega)^4} \times \left[2a_j^2 \frac{3\omega_{0,j}^2 - 8\omega^2 - 8\gamma i \omega}{\omega_{0,j}^2 (\omega_{0,j}^2 - 4\omega^2 - 4\gamma i \omega)} + 3b_j \right]. \quad (\text{S8})$$

The nonlinear absorption coefficient is related to the complex nonlinear refractive index as

$$\alpha_2 = 2 \frac{\omega}{c} \Im(\tilde{n}_2) \quad (\text{S9})$$

Figure S1 shows the dispersion of the nonlinear absorption coefficient caused by the dominant resonance and the resonances at 7.9 THz and 3.9 THz. The top inset of of Figure (S1) resolves the value of α_2 at around low-frequency resonances. The comparison indicates that the nonlinear absorption coefficient at the dominant resonance at 37.2 THz is approximately 100 times larger than the one at the strongest resonance of the two lower-frequency resonances. The value of the nonlinear absorption coefficient at 0.4 THz is $\alpha_2 \approx 1.49 \times 10^{-10} \text{ m W}^{-1}$, which has a slight difference with the measured data (a factor of 1.84).

Data analysis

The spectral density of the THz field is shown in Figure S2 (a), where the squares of the magnitude of fast Fourier transform (FFT) of time-domain signals are displayed. The temporal signal is also zero-padded so that we have smoother frequency response. The total absorption of the sample with thickness of L can be calculated as the ratio between the magnitude of the FFT signals of quartz $|E_q(\omega)|$ and free-space $|E_f(\omega)|$, after factoring out Fresnel reflections, becomes

$$e^{-\frac{\alpha}{2}L} \times |R_{Fr}|^2 = \frac{|E_q(\omega)|}{|E_f(\omega)|}, \quad (\text{S10})$$

where the $R_{Fr} = \frac{n_{\text{quartz}} - 1}{n_{\text{quartz}} + 1}$ is the Fresnel coefficient. Thus, the absorption coefficient is given by

$$\alpha = -\frac{2}{L} \ln \left(\frac{1}{|R_{Fr}|^2} \frac{|E_q(\omega)|}{|E_f(\omega)|} \right). \quad (\text{S11})$$

The nonlinear phase of each signal level with respect to the lowest-level signal is shown in Figure S2 (b).

References

- [1] K. Dolgaleva, D. V. Materikina, R. W. Boyd, S. A. Kozlov, *Phys. Rev. A* **2015**, *92* 023809.
- [2] C. Tan, *Journal of Non-Crystalline Solids* **1998**, *223*, 1 158.
- [3] See THz Material data sheet, https://www.tydexoptics.com/products/thz_optics/thz_materials.
- [4] C. L. Davies, J. B. Patel, C. Q. Xia, L. M. Herz, M. B. Johnston, *Journal of Infrared, Millimeter, and Terahertz Waves* **2018**, *39*, 12 1236.